Nucleophilic Substitution Reactions at Liquid/Liquid Interfaces: Molecular Dynamics Simulation of a Model S_N1 Dissociation Reaction at the Water/Carbon Tetrachloride Interface

Nicole Winter and Ilan Benjamin*

Department of Chemistry, University of California, Santa Cruz, California 95064

Received: April 22, 2005; In Final Form: June 28, 2005

The ionic dissociation step of the nucleophilic substitution reaction *t*-BuCl → *t*-$Bu^+ + Cl^-$ is studied at the water/carbon tetrachloride interface using molecular dynamics computer simulations. The empirical valence bond approach is used to couple two diabatic states, covalent and ionic, in the electronically adiabatic limit. The umbrella sampling technique is used to calculate the potential of mean force along the reaction coordinate (defined as the *t*-Bu to Cl distance) at several interface regions of varying distances from the Gibbs dividing surface. We find a significant increase of the ionic dissociation barrier height and of the reaction free energy at the interface relative to bulk water. This is shown to be due to the reduced polarity of the interface which causes a destabilization of the pure ionic state. However, deformation to the neat interface structure in the form of water protrusions into the organic phase may provide partial stabilization of the ionic species. The importance of these structural effects is examined by repeating the calculations with an artificially smooth interface. The destabilization of the ionic state at the interface also manifests itself with a rapid (picosecond time scale) recombination dynamics of the ions to form the parent molecule followed by a slow vibrational relaxation.

I. Introduction

The study of chemical reactions at liquid interfaces has great fundamental importance and is also directly relevant to many practical applications. The inhomogeneous environment at the interface gives rise to a number of unique properties that can influence the rate and energetics of chemical reactions and cause significant deviations from bulk behavior. Gaining insight into the effects of surface polarity, solvent clustering, and surface roughness on chemical reactions may improve understanding of the chemistry at liquid/liquid interfaces. This fundamental understanding is important for applications such as drug delivery methods in pharmacology[1] and environmental concerns including uptake of pollutants by water surfaces.[2] Industrial examples that include liquid interfaces are photoelectrochemical cells, liquid chromatography, and phase transfer catalysis[3] (PTC). PTC, which has great practical importance for the synthesis and manufacture of numerous organic compounds,[3] involves reactions that take place at or near the interface between water and an organic solvent. Much recent interest has also focused on reactions that take place inside micelles and in microemulsions. While the large effective surface areas in these systems facilitate the study of interfacial reactions, at the molecular level these systems present an environment that is very similar to that at the liquid/liquid interface. Examples of PTC reactions and reactions in microemulsions studied in recent years include the following: solvolysis of substituted benzoyl chloride at the water/isooctane interface,[4] formation of carbene chloride by abstraction of a chloride ion from a carbon trichloride anion in water/cyclohexene microemulsions,[5] and the nucleophilic substitution reaction of decyl bromide with the sulfonate anion in different water/oil microemulsions.[6]

An important class of reactions that has been the focus of several recent experimental studies at interfaces are reactions that involve a significant change in the molecular charge distribution of the reactants and products. In addition to the reactions mentioned in the end of the last paragraph, other examples include the study by Corn and co-workers, who used second harmonic generation (SHG) to examine the acid−base equilibrium of an azobenzene surfactant at the water/1,2-dichloroethane interface,[7] and the study by Sawada and co-workers, who used time-resolved quasi-elastic laser scattering (QELS) to monitor the dynamics of a phase transfer catalytic reaction system involving quaternary ammonium bromide, $R_4N^+Br^-$ (R = *n*-C_4H_9, *n*-C_3H_7, *n*-C_2H_5).[8] While many theoretical studies of these reactions have been carried out in bulk solutions,[9−15] very little is known or has been done to investigate the effect of an inhomogeneous surface environment on these reactions.

In this paper we present a detailed study of the dissociation step of a model S_N1 reaction at the water/carbon tetrachloride interface. Specifically, we consider the dissociation of *tert*-butyl chloride (*t*-BuCl). This is an important case to examine because it has been studied both experimentally[16,17] and theoretically[18−23] in bulk liquids, including very recently in supercritical water.[24] Reasonably accurate potential energy surfaces are available, and the insight gained about interfacial effects on this system can be compared to the bulk results. Our goal is to understand how the unique interfacial properties influence the thermodynamics and dynamics of *t*-BuCl dissociation. In particular, we focus on two important characteristics of the liquid/liquid interface: its polarity and its dynamic roughness.

Recent solvatochromic shift measurements of adsorbed dye molecules at liquid/liquid interfaces[25,26] have demonstrated that the polarity of the interface between water and non-hydrogen bonding solvents varies monotonically across the interface, whose width is estimated to be only a few nanometers wide.

10.1021/jp052112o CCC: $30.25
Published on Web 08/05/2005

We demonstrate that this "polarity profile" manifests itself in the reaction free energy profile by computing the potential of mean force (PMF) for the reactants located in various locations along the interface normal. Since it is well-known that solvent polarity has a dramatic effect on the rate and yield of this reaction in bulk water, we expect the anisotropic polarity of the interface to play a major role. Specifically, reducing solvent polarity destabilizes the ionic potential energy surface, creates a larger activation barrier to dissociation, and shifts the transition state location to larger values of the *t*-Bu−Cl bond distance. Molecular dynamics simulations[27−29] and indirect experimental evidence[30,31] suggest that although the interface between two immiscible liquids is quite sharp (so the polarity may change quite abruptly), thermally excited density fluctuations at the interface can create dynamic surface roughness which may provide unexpected stabilization of ionic species. For example, it has been shown that a water "finger" consisting of several water molecules protruding into the organic phase may be formed due to thermal fluctuations at the interface.[32] This water "finger" can interact with an ion on the organic side of the interface and affect the barrier to ion transfer across the interface.[32] Similarly, such surface roughness can markedly influence the free energy change for dissociation of *t*-BuCl to ions, even when the solute is deep in the organic phase.

The remainder of this paper is organized as follows. Section II provides details of the simulations including descriptions of the potentials, the system, and the methodology. In section III we discuss the results of the free energy calculations in light of the surface roughness and the solvent shell structures. We also discuss briefly the results of recombination dynamics calculations of *t*-BuCl at the water/CCl_4 interface. Last, we conclude in section IV with a summary and note of future directions that will build on this work.

II. Simulation Details

In this section we outline the potential energy functions for the system, the setup of the system, and the methodology for all of the PMF calculations.

A. Empirical Valence Bond Approach. We use a two-state empirical valence bond (EVB) model to describe the *t*-BuCl molecule.[15,20,22,33−36] The total wave function is written as a linear combination of two diabatic states, one covalent and one ionic:

$$\Psi = c_{\mathrm{cov}}\psi_{\mathrm{cov}} + c_{\mathrm{ion}}\psi_{\mathrm{ion}} \tag{1}$$

Diagonalization of the total Hamiltonian yields the electronic ground state energy in the adiabatic approximation as a function of all nuclear coordinates. This adiabatic Hamiltonian is used for describing the classical motion of the system in the ground state and is given by

$$H_{\mathrm{ad}} = E_{\mathrm{k}} + \frac{1}{2}(U_{\mathrm{cov}} + U_{\mathrm{ion}}) - \frac{1}{2}[(U_{\mathrm{cov}} + U_{\mathrm{ion}})^2 + 4U_{\mathrm{coup}}{}^2]^{1/2} \tag{2}$$

U_{cov} and U_{ion} are the total potential energies of the system when the *t*-BuCl is in the covalent and ionic states, respectively. $U_{\mathrm{cov}} = u_{\mathrm{cov}} + u_{\mathrm{cov-W}} + u_{\mathrm{cov-CTC}} + u_{\mathrm{W}} + u_{\mathrm{CTC}} + u_{\mathrm{W-CTC}}$ includes in the order, from left to right, the gas-phase covalent potential for the *t*-Bu and Cl radical pair, their interaction with water, their interaction with carbon tetrachloride (CCl_4), the water potential (intramolecular and intermolecular), the CCl_4 potential (intramolecular and intermolecular), the water−CCl_4 intermolecular potential. $U_{\mathrm{ion}} = u_{\mathrm{ion}} + u_{\mathrm{ion-W}} + u_{\mathrm{ion-CTC}} + u_{\mathrm{W}} + u_{\mathrm{CTC}} + u_{\mathrm{W-CTC}} + \Delta E_{\mathrm{offset}}$ includes the gas-phase ionic potential for the *t*-Bu^+ and Cl^- ions, their interaction with water, their interaction with CCl_4, the water potential (intramolecular and intermolecular), the CCl_4 potential (intramolecular and intermolecular), the water−CCl_4 intermolecular potential, and an offset term that accounts for the electron affinity of Cl plus the ionization energy of *t*-Bu. U_{coup} is the electronic coupling between the two states, which has an exponential dependence on the *t*-Bu−Cl distance *R*.

TABLE 1: Lennard-Jones and Coulomb Atomic Parameters

atom (in molecule)	σ (Å)	ϵ (kcal/mol)	q (au)
O (H_2O)	3.1655	0.1554	−0.8476
H (H_2O)	0	0	0.4238
C (CCl_4)	4.6	0.1	0.2
Cl (CCl_4)	3.5	0.19	−0.05
Cl (*t*-BuCl)	3.35	0.3448	0
Cl^- (*t*-BuCl)	4.417	0.118	−1
t-Bu (*t*-BuCl)	5.3304	0.1695	0
t-Bu^+ (*t*-BuCl)	5.3304	0.1695	1

B. Potentials and Parameters. The potentials for the solute and solute−water interactions are mostly taken from a recent study of *t*-BuCl in supercritical water by Westacott et al.[24] These potentials are modified by the addition of the CCl_4 solvent.

1. Solute Potentials. The parametrization of the Hamiltonian given in eq 2 is done by a fit to experimental and ab initio data.[24] The *t*-Bu species is represented by a central carbon with three surrounding united atom methyl (Me) groups, attached at a fixed distance $r_{\mathrm{CMe}} = 1.475$ Å in a planar trigonal geometry perpendicular to the carbon−chloride bond. Each of the three Me−Cl bond distances is related to *R* via $r_{\mathrm{MeCl}}{}^2 = r_{\mathrm{MeCl}}{}^2 + R^2$. The gas-phase pure ionic state $u_{\mathrm{ion}}(R)$ is given by a sum of an exponential repulsion term, an induced dipole attractive term (R^{-6}), and a Coulomb term for the interactions between the central carbon atom and the three methyl groups with the chloride ion. The gas-phase pure covalent state $u_{\mathrm{cov}}(R)$ is described by a Morse potential. The explicit forms for $u_{\mathrm{ion}}(R)$ and $u_{\mathrm{cov}}(R)$ (including the detailed parametrization) have been discussed previously.[24,37]

2. Solvent Potentials. The water potential is described by a fully flexible simple point charge (SPC) model that we have utilized extensively in the past, which includes the intramolecular potential of Kuchitsu and Morino.[38] The CCl_4 intermolecular potential is a five-site all-atoms model with Lennard-Jones plus Coulomb interactions between the sites with parameters given in Table 1. The intramolecular potential includes bond stretching (force constant = 4.38 (kcal/mol)/Å; equilibrium bond length = 1.77 Å) and angle bending harmonic terms (force constant = 0.331 (kcal/mol)/rad, tetrahedral equilibrium bond angle). These models for water and CCl_4 give reasonable bulk and interfacial properties.[39−41] Note that the large polarizability of the CCl_4 molecule is taken into account only through the use of effective pair potentials. In recent years, the effect of many-body polarizable potentials on the structure and dynamics of condensed bulk[42−49] and interfacial systems[50−55] has been the focus of many studies. While the incorporation of a polarizable intermolecular potential into the EVB approach should not pose a difficult problem, we postpone this to future studies and only note here that the increase in the local dipole moment of interfacial CCl_4 molecules[52] is expected to provide somewhat additional stabilization to the ion pair at the interface.

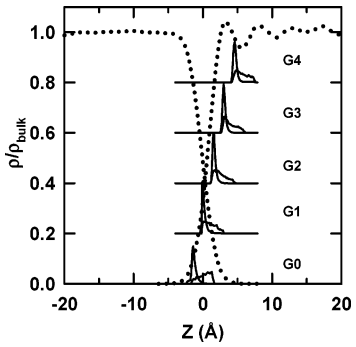

Figure 1. Density profiles (dotted lines) of water ($Z < 0$) and CCl_4 ($Z > 0$) at liquid/liquid interface. Superimposed are the probability distributions of the *t*-BuCl center-of-mass position in the different regions (labeled G0−G4) near the interface. The short, broad distributions and the tall, narrow distributions represent the probability distribution when the *t*-BuCl is covalent and ionic, respectively.

3. Solvent−Solute Potentials. The solute−solvent intermolecular potential is represented by a pairwise sum of Lennard-Jones and Coulomb terms:

$$u_{ij}(r) = 4\epsilon_{ij}\left[\left(\frac{\sigma_{ij}}{r}\right)^{12} - \left(\frac{\sigma_{ij}}{r}\right)^{6}\right] + \frac{q_i q_j}{4\pi r \epsilon_0} \qquad (3)$$

where "*i*" and "*j*" denote atoms on two different molecules separated by a distance *r*. The solute is treated as a two-site species, with the *t*-Bu group described as a united atom. Different parameters are used in the potential energy functions when the solute is in the ionic or covalent state. The intermolecular parameters for the solute in the covalent and ionic states, as well as for the water and CCl_4 solvents, are given in Table 1. Note that in this work the standard mixing rules,[56] $\epsilon_{ij} = \sqrt{\epsilon_i \epsilon_j}$ and $\sigma_{ij} = (1/2)(\sigma_i + \sigma_j)$, are used for the Lennard-Jones parameters between different sites.

C. Methods. All molecular dynamics (MD) simulations in this work are done with a 0.5 fs time step using the velocity version of the Verlet algorithm at 298 K.

1. System Preparation. The system includes 500 water and 213 CCl_4 molecules in a rectangular box of dimensions $L_x = L_y = 24.83$ Å $< L_z = 200$ Å. The density profiles of water and CCl_4 near the liquid/liquid interface region calculated from a 2 ns molecular dynamics trajectory at 298 K are shown in Figure 1. The Gibbs surface (near $Z = 0$) is the plane perpendicular to the interface normal where the water density is 50% of the bulk value. To investigate the full range of interfacial effects, we allow the *t*-BuCl solute to sample one of five regions along the interface normal. These regions are defined as follows:

region G0: -1.5 Å $< Z <$ 1.5 Å

region G1: 0.0 Å $< Z <$ 3.0 Å

region G2: 1.5 Å $< Z <$ 4.5 Å

region G3: 3.0 Å $< Z <$ 6.0 Å

region G4: 4.5 Å $< Z <$ 7.5 Å

The solute is inserted and equilibrated in one of the above regions in preparation for the calculation of the PMF. To increase the sampling statistics, the solute is restricted to each region by a window potential acting on the solute center-of-mass coordinate Z_{cm}:

$$u_{win}(Zc_m) = kH(\zeta)\zeta^3; \qquad \zeta = |Z_{cm} - c| - w/2 \qquad (4)$$

where c is the center of the window, $w = 3$ Å is its width, and $H(\zeta)$ is the unit step function: $H(\zeta) = 0$ for $\zeta \le 0$ and $H(\zeta) = 1$ for $\zeta > 0$. Included in Figure 1 are the superimposed probability distributions of the solute center of mass in the different locations along the liquid/liquid interface.

The solute distributions are obtained from the long equilibrium runs used to calculate the PMF along the reaction coordinate *R*. In each of the five regions we show two solute position probability distributions. The broader peaks correspond to mostly covalent *t*-BuCl, and the taller, narrower peaks correspond to mostly ionic *t*-BuCl. Notice that the taller ionic peaks are shifted strongly toward the water. This difference is due to the strong interaction of the more ionic *t*-BuCl with the highly polar water. This will be discussed further below.

2. Potential of Mean Force. The PMF calculations are done with the solute confined to one of five regions located near the liquid/liquid interface as described above. The PMF is related to the probability distribution along the reaction coordinate via

$$W(R) = -kT \ln P(R) \qquad (5)$$

where *R* is the distance between the chlorine and the central carbon in the *tert*-butyl species. To improve statistical sampling, we use the method of overlapping windows. This is done by dividing the range of relevant values of *R* to eight 0.4-Å-wide windows from $R = 1.4$ Å to $R = 3.9$ Å such that every pair of neighboring windows has a 0.1 Å overlap. A simple harmonic potential is used to keep the solute in the range of the window. $P(R)$ is determined from 250 ps of equilibrium MD in each window. Because $W(R)$ changes significantly as a function of *R* in the region 1.4 Å $< R <$ 2.4 Å, direct sampling of $P(R)$ is impossible. We use a non-Boltzmann preferential sampling by adding a biasing potential, $U_b(R)$, to the total Hamiltonian to ensure that the full range of the window is adequately visited. The PMF can then be calculated as follows:

$$W(R) = -kT \ln P_b(R) - U_b(R) \qquad (6)$$

where $P_b(R)$ is the probability distribution calculated with the biased Hamiltonian. A sixth degree polynomial fit to the PMF result for the lowest density region of the water liquid/vapor interface as calculated in the previous study[37] works well as a biasing potential for sampling at the water/CCl_4 interface because of the similarities between these two systems. Due to the very weak interaction between *t*-BuCl and CCl_4, a polynomial fit to the gas phase *t*-BuCl adiabatic potential serves as the biasing potential for determining the PMF in bulk CCl_4.

Ionic PMF. Since the main influence on the PMF when water is present is due to changes in the pure ionic potential, we calculate the PMF curves for *t*-Bu^+ and Cl^- ions in each interfacial region. The methods are the same as described above for the adiabatic *t*-BuCl free energy calculations; however, the sampling is done solely with the ionic potential and ionic interactions with the solvent instead of the adiabatic potential of eq 2. Due to significant changes in the free energy for small *t*-Bu−Cl distances, a biasing potential is employed in this region. The biasing potential is based on a fit to the PMF of the ions in bulk water as obtained from statistical mechanical perturbation theory calculations. For details on this method, see ref 57. The perturbation theory method is also used to calculate the covalent PMF in bulk water, which will be discussed along with the ionic PMFs in section III.

PMF with "Flat" Interface. As mentioned in section I, the interface structure, and in particular surface roughness, may significantly alter the PMF relative to what it would be if the

interface were perfectly flat. To examine this, we repeat the PMF calculations in each region, keeping the water/CCl_4 interface flat via a simple harmonic potential function of the center-of-mass coordinate ($z_{i,cm}$) of each solvent molecule "*i*":

$$u_i(z_{i,cm}) = kH(\zeta)\zeta^2; \quad \zeta = z_{i,cm} \text{ for water}, \quad \zeta = -z_{i,cm} \text{ for } CCl_4 \quad (7)$$

where $H(\zeta)$ is the unit step function as defined above and the interface is assumed to be at $z = 0$.

3. Solvation Free Energy. The PMF gives the free energy as a function of R up to an additive constant. To set the free energy curves relative to each other, we set the free energy at the largest R value sampled, R_{max}, according to

$$W(R_{max}) = u_{ion}(R_{max}) + \Delta A_{solv}(R_{max}) \quad (8)$$

where $u_{ion}(R_{max})$ is the value of the gas-phase ionic *t*-BuCl potential at R_{max} and $\Delta A_{solv}(R_{max})$ is the calculated solvation free energy for the *t*-Bu^+ and Cl^- ions a distance R_{max} apart in the corresponding region.

4. Free Energy for Transfer across the Interface. To determine the change in free energy of the solute as a function of the distance from the interface, we sample the probability distribution $P(Z_{cm})$, where Z_{cm} is the center-of-mass coordinate of the solute along the *Z*-axis. We do this for two cases: (1) R fixed at the PMF well minimum (1.75 Å) and (2) R fixed at the contact ion pair (CIP) minimum as determined from the PMF in the G0 region (2.7 Å). We again used the method of overlapping windows to do the sampling: eight 3-Å-wide windows in the *Z*-direction spanning the region from $Z = -8$ Å (bulk water) to $Z = 9$ Å (bulk CCl_4), such that every two windows have a 1 Å overlap. A 250 ps equilibrium MD trajectory in each window yields $P(Z_{cm})$, and the free energy change can be calculated from

$$A(Z) = -kT \ln P(Z_{cm}) \quad (9)$$

5. Recombination Dynamics. Because of the large barrier to dissociation, direct observation of thermally excited dissociation trajectories is impossible. Instead, we examine the recombination dynamics of the ions in the regions closest to the organic phase. Nonequilibrium MD trajectories were performed with the *t*-Bu^+ and Cl^- ions initiated 3 Å apart in either the G2, G3, or G4 interfacial regions. The *t*-Bu−Cl distance R is monitored at 5 fs intervals during a 10 ps trajectory. We use 10 independent configurations of the system as seed files, running 10 trajectories from each seed file, all with random initial velocities drawn from a Boltzmann distribution, yielding 100 trajectories in each of the three regions. We obtain the probability distribution $P(R)$ as a function of time by binning the R values between the following time intervals: 0−50 fs, 50−200 fs, 0.2−1 ps, 1−2 ps, and 9−10 ps.

III. Results and Discussion

Before examining the reaction free energy profile at a liquid/liquid interface, we consider the surface activity of the parent molecule and of the products. Figure 2 shows the free energy change as a function of distance from the Gibbs surface ($Z = 0$) for the bound *t*-BuCl molecule at its equilibrium configuration (dashed line) and for the contact ion pair held fixed at $R = 2.7$ Å (dotted line).

We find that the bound solute free energy decreases (starting at $Z = -5$ Å) by 4 kcal/mol upon moving from bulk water to the Gibbs surface, and then slightly increases as it is moved into bulk CCl_4, indicating that the parent molecule is surface active. In contrast, there is a 17.5 kcal/mol barrier to the transfer of the CIP from the aqueous to the organic phase. It is interesting to note that the free energy profile begins to rise only as the CIP crosses the Gibbs surface, suggesting that it is substantially hydrated at that location. The profile levels off near $Z = 8$ Å in the bulk CCl_4 region. Clearly the CIP (with $|c_i| = 1$ regardless of Z location) is more stable in the highly polar water solvent. The reaction free energy or the potential of mean force (PMF) curves for *t*-BuCl in the five interface regions, bulk water, and bulk CCl_4 are shown in Figure 3 (bottom panel). For comparison, the top panel depicts the gas-phase ionic, covalent, and adiabatic potential energy functions.

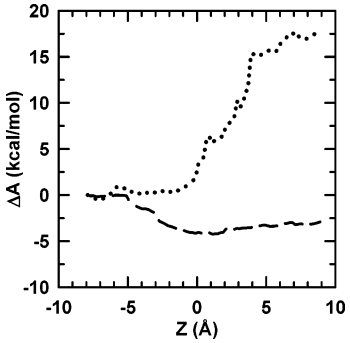

Figure 2. Free energy change for transfer of *t*-BuCl from the aqueous to the organic phase. The *t*-Bu-Cl bond distance is fixed either at the ground state minimum (dashed line) or at the contact ion pair distance, $R = 2.7$ Å (dotted line).

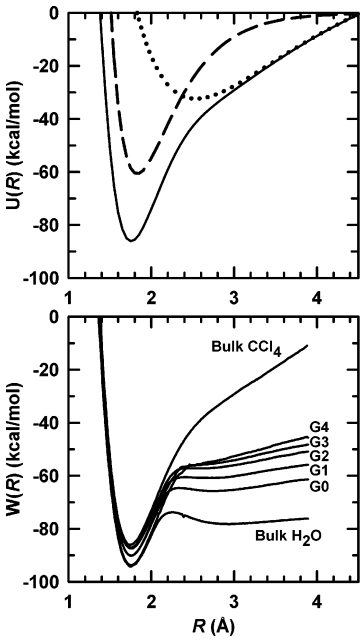

Figure 3. Potential of mean force of *t*-BuCl in bulk water, bulk CCl_4, and each interface region (bottom panel) compared with the gas-phase potentials (top panel; solid, dashed, and dotted lines correspond to adiabatic, covalent, and ionic states, respectively).

As mentioned in section IIC, the curves are set relative to each other according to the solvation free energy of the ions in each region (see eq 8). Therefore, when the interionic distance is 3.9 Å in bulk water, the free energy is −76 kcal/mol relative to the gas-phase covalent molecule. The PMF in bulk water is generally in agreement with previous calculations.[21,24] The minimum lies at a *t*-Bu−Cl separation of $R = 1.75$ Å and the transition state to dissociation lies at $R = 2.24$ Å with a barrier height of 20.5 kcal/mol relative to the bound well minimum,

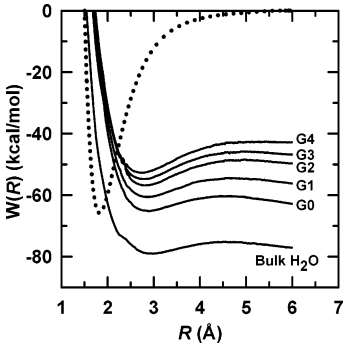

Figure 4. Potential of mean force for *t*-Bu^+ and Cl^- ions in bulk water and in each interface region. The potential of mean force for the covalent *t*-BuCl in bulk water is shown for comparison by the dotted line.

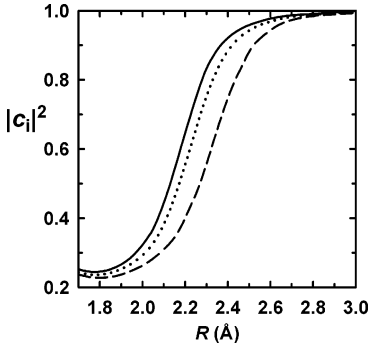

Figure 5. Ionic character vs solute bond length R at water/CCl_4 interface. The solid, dotted, and dashed lines correspond to the G0, G2, and G4 regions, respectively.

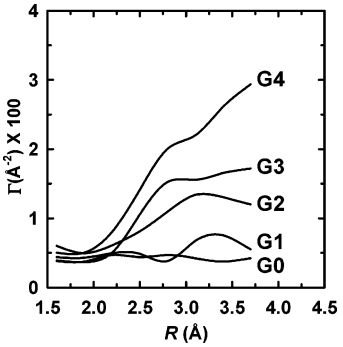

Figure 6. Water surface excess (eq 10) as a function of *t*-Bu−Cl distance for the solute in each of the five interface regions.

which is in good agreement with experiment.[58] We also note that the absolute vertical shift of the bulk PMF curve is in excellent agreement with previous calculations.[24] We note the following points regarding the interfacial PMF curves:

(1) The location of the PMF minimum remains at $R = 1.75$ Å regardless of the location of the *t*-BuCl solute relative to the interface.

(2) As the solute is transferred to the organic phase, the transition state moves to slightly larger R values, from $R = 2.33$ to 2.41 Å, and the barrier height increases from 25.5 to 26.9 kcal/mol in the G0 and G1 regions, respectively.

(3) The CIP minimum becomes shallower relative to the transition state and moves to smaller interionic separations as the solvent environment becomes less polar. This applies only to the G0 and G1 regions, as the CIP is no longer stable in the G2, G3, and G4 regions ($Z > 3$ Å).

We can attribute all of the above characteristics to the stabilization of the ionic state by the solvent, with the covalent potential remaining similar to that in the gas phase. The more polar the solvent, the more stabilization afforded to the ions. We demonstrate this quantitatively by computing the pure ionic state PMF curves in bulk water and in the five interfacial regions. The curves are set vertically according to eq 8 and are shown in Figure 4. The covalent PMF curve for *t*-BuCl in bulk water is shown by the dotted line for reference. Note that since the solvation free energy of the *t*-Bu and Cl radicals is only a few kilocalories per mole and furthermore is expected to vary only slightly between the different regions, we can safely neglect it and set $W(R) = 0$ as $R \rightarrow \infty$ for the covalent PMF.

As the ion pair location is shifted from bulk water to bulk CCl_4, the polarity of the solvent environment decreases and we note the following trends in the ionic PMF curves:

(1) The ionic state becomes less stabilized relative to bulk water.

(2) The crossing point between the ionic and covalent curves moves to higher energy and larger R separation. The ionic/covalent crossing point essentially determines the transition state location in the adiabatic PMF curve. This shifting of the crossing point is consistent with the trends noted above for the transition state, namely the shifting to larger R values and increase in activation barrier height with a decreasingly polar environment.

(3) The minimum in the ionic PMF (which corresponds to the CIP minimum in the adiabatic PMF) moves to smaller interionic separations. This is consistent with the trend for the CIP minimum in the adiabatic PMF curves.

In Figure 5 we show the ionic character as a function of R. The observed trend is consistent with the increased stabilization of the ionic state as R increases and as the solute is moved closer to the aqueous phase. The ionic character increases monotonically from $|c_i| = 0.25$ near the reactant well minimum to near $|c_i| = 1$ at the contact ion pair minimum, with the main difference being the faster rate at which the ionic character changes as *t*-BuCl crosses the transition state for regions of higher polarity.

It is interesting that the destabilization of the ionic PMF curves (and the adiabatic PMF curves) is not more dramatic upon moving the solute from the G0 to G4 regions (the most polar to least polar regions). The G4 region is located well into bulk CCl_4 according to the density profile of the neat water/CCl_4 interface, but we still observe significant stabilization of the ions relative to the gas phase. We find this to be due to water molecules moving into the CCl_4 phase, particularly when the ionic character is large. Insight into this stabilization is given in Figure 6, which shows the water surface excess Γ as a function of the *t*-Bu−Cl distance R. Γ is defined as

$$\Gamma = \int_{Z_G}^{\infty} (\rho - \rho_0)\, dz \qquad (10)$$

where Z_G is the Gibbs dividing surface, ρ is the density profile in the presence of a solute, and ρ_0 is the neat water/CCl_4 density profile.

Two details that are clear from the figure are that (1) the water excess (relative to the neat interface) increases with increasing ionic character of the *t*-BuCl and (2) this increase is more dramatic as the *t*-BuCl is moved further into the organic phase. This indicates that the water is essentially being dragged over to the CCl_4 side, which accounts for the stability of the ions even in the G4 region. This suggests that the local solvent environment around the ions in regions G0 and G4 is similar, and this is consistent with the observation that the solvation free energies in the G0 and G4 regions are somewhat similar.

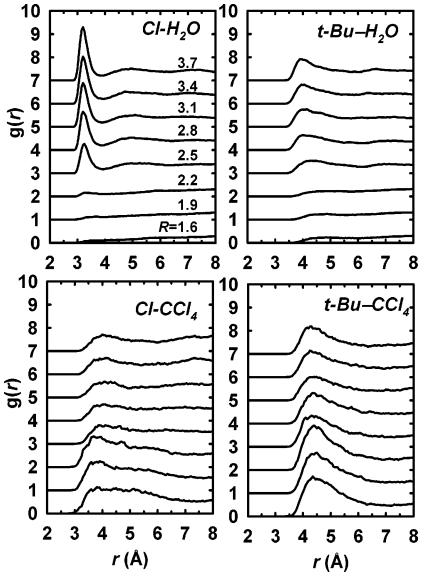

Figure 7. Solute to solvent radial distribution functions (RDFs) in the G2 region for various separations along the reaction coordinate (as indicated in the top left panel). The RDFs are measured from Cl or *t*-Bu to O(H_2O) or C(CCl_4) as labeled in each panel.

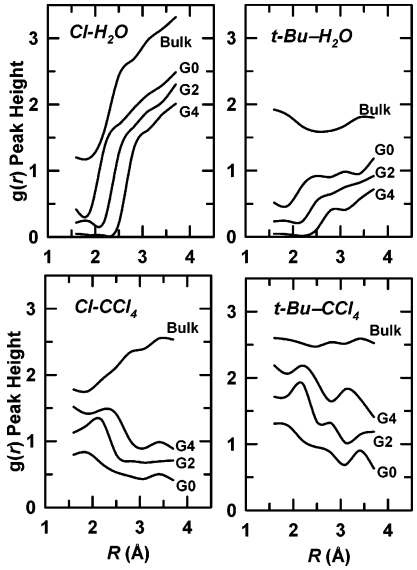

Figure 8. First solvation shell peak heights of RDFs shown in Figure 7 as a function of *t*-Bu−Cl separation. We omit regions G1 and G3 for clarity.

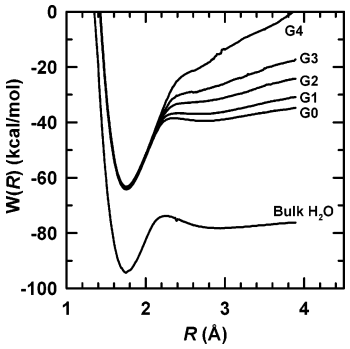

Figure 9. *t*-BuCl potential of mean force calculated in each interfacial region with the interface forced to be flat. The PMF in bulk water is shown for comparison.

To quantify the change in the local solvent environment as a function of the reaction coordinate, Figure 7 shows the solute to solvent radial distribution functions (RDF) for various separations R of *t*-Bu and Cl in the G2 region (the RDF shapes are similar for all interfacial regions, so we show G2 as the example). Note that these are calculated from the adiabatic ground state simulations.

Let us focus first on the Cl−H_2O RDF in the upper left panel of Figure 7: Similar to bulk water, no clear first water solvation shell peak is observed until the transition state is reached. At this point, as the ionic character rapidly increases, there is a sudden formation of the first peak at $r = 3.2$ Å. The height of the first solvent peak increases with increasing ion separation while a small broad peak, near $r = 5$ Å, marking the second solvation shell, also appears. The lower left panel of Figure 7 shows analogous RDF plots for Cl−CCl_4. Notice that the first CCl_4 solvation shell peak decreases with increasing ion separation, due to displacement by water molecules coming in to stabilize the ions. The upper right and lower right panels of Figure 7 show the RDF plots for *t*-Bu with water and CCl_4, respectively. Again, these plots reflect the water solvent shell peak increasing while the CCl_4 solvent shell peak decreases with increasing ion separation. Note that the *t*-Bu−H_2O peak heights are shorter than the corresponding Cl−H_2O peak heights, whereas the trend is opposite for the *t*-Bu−CCl_4 and Cl−CCl_4 RDF plots (the *t*-Bu−CCl_4 peak heights being larger) due to *t*-Bu being a hydrophobic ion. Figure 8 shows the first solvent peak height as a function of the *t*-Bu−Cl separation R in the bulk compared with that in the G0, G2, and G4 interfacial regions.

These curves more clearly show the movement of water into the first solvation shell around the two ions, while displacing the CCl_4. The *t*-Bu ion has little change in its solvation shell with increasing ionic character in either bulk water or bulk CCl_4, whereas the solvent density increases around the Cl species with increasing ionic character in both bulk solvents due to its much greater charge density (and lack of hydrophobicity).

It is clear that the change in interface structure due to water following the solute into the organic phase has a major effect on the PMF. To quantify this, we repeated the calculations of the adiabatic PMF in each interfacial region with the interface forced to be flat, and the results are shown in Figure 9.

Although removing the surface roughness has little effect on the shape of the PMF curves, we find that the curves are shifted upward due to the smaller solvation free energy. Also, the slope of the PMF beyond the transition state is larger (more positive), indicating that the formation of ions is less favored without the ability of the water to move in and provide stabilization. This is most significant in the G4 region, where the PMF is essentially the same as in bulk CCl_4 if the interface is held flat.

It is instructive to compare some of our findings to the results of similar calculations in supercritical water[24] and at the water liquid/vapor interface.[37] In all the cases, as the medium becomes less polar, the nature of the PMF changes in a similar way: The barrier to dissociation increases, its location moves to larger interionic distances, and the stability of the products diminishes. However, in all systems the effect seems to be less than one would expect based on the dramatic drop in polarity. This has been explained in terms of local density enhancement in supercritical water and at the water liquid/vapor interface, while in the present system it is due to surface deformation. However, this surface deformation can also be viewed as a mechanism that enables the ions to increase their interactions with the water.

Finally, we briefly consider the recombination dynamics. The potential of mean force can be used to compute an estimate of the rate constant to dissociation or recombination. In bulk water

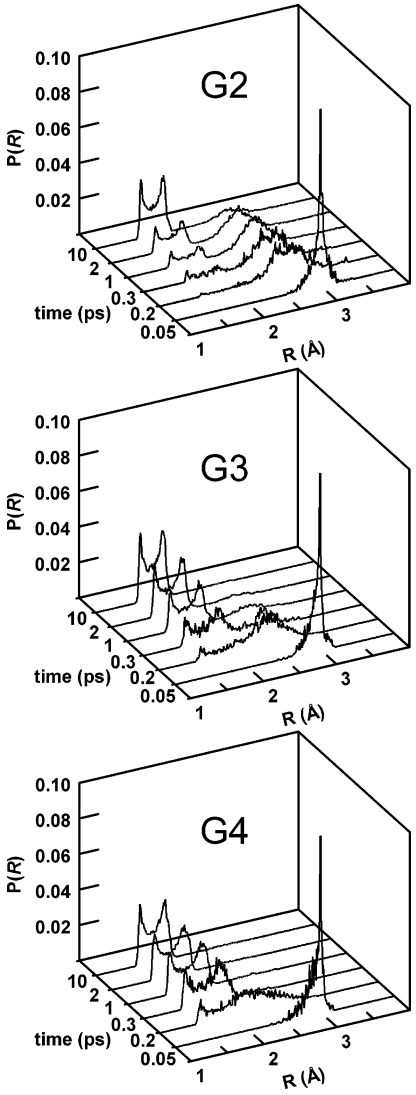

Figure 10. Recombination dynamics in G2, G3, and G4 regions (as labeled) shown by probability distributions of the *t*-Bu−Cl distance *R* as a function of time for *t*-BuCl initiated at $R = 3$ Å.

there is a well-defined transition state and the rate constant can be written for the bimolecular reaction as

$$k = (k_B T/h) \exp[-E_a/k_B T] \qquad (11)$$

where k may be calculated by initiating trajectories at the transition state and calculating the fraction that recross the barrier. However, since the product well for formation of the CIP is very shallow at the interface (as in the G0 and G1 regions) or nonexistent (as in the G2, G3, and G4 regions), there is no well-defined transition state. Instead, we investigated the recombination dynamics for *t*-BuCl initiated near the CIP distance ($R = 3$ Å) in regions where the PMF has no CIP free energy minimum. The probability distribution of R as a function of time is shown in Figure 10 for the G2, G3, and G4 regions.

By 50 fs the $P(R)$ distribution in all three regions begins to spread over a distance of ~0.5 Å and shift toward smaller R values. By 200 fs, a significant number of trajectories reach the covalent well minimum in the G4 region, fewer in the G3 region, and very few in the G2 region. The more rapid recombination in the G3 and G4 regions can be attributed to the steeper PMF curve in these less polar regions, which reflects the less favorable solvation of the ions in these regions. By 1 ps, essentially all of the trajectories have been trapped in the covalent well in the less polar G3 and G4 regions while only about half the trajectories in the G2 region have been trapped. The other half remain near the CIP distance, but by 10 ps, 80% of the total number recombine. This is in contrast to the 100% recombination in the G3 and G4 regions by 10 ps. In all three regions the recombined *t*-BuCl remains vibrationally hot at 10 ps. The slower relaxation at the interface (relative to bulk water) is consistent with previous studies of vibrational relaxation at interfaces.[59−61]

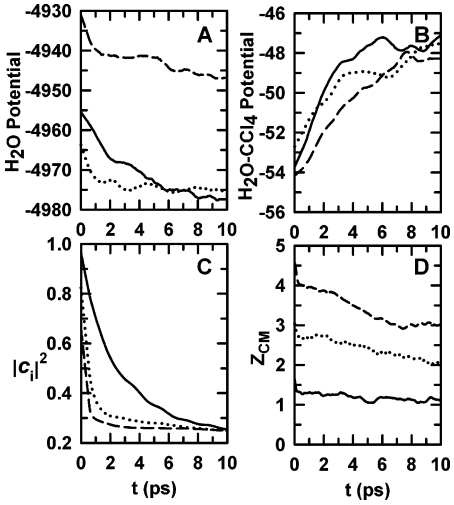

Figure 11. Ensemble averages of water potential energy (A), water−CCl_4 potential energy (B), solute ionic character (C), and center-of-mass distance Z from the Gibbs dividing surface (D) during the recombination dynamics. The solid, dotted, and dashed lines correspond to the G2, G3, and G4 regions, respectively. Energies are in kcal/mol, and distances are in Å.

Additional insight into the recombination process is provided in Figure 11, which shows the average water potential energy (panel A), the average water−CCl_4 potential energy (panel B), the solute ionic character (panel C), and the solute atom positions relative to the Gibbs surface during the recombination in all three interfacial regions (Panel D). The rapid decrease in ionic character of the solute as it recombines in regions G3 and G4 compared with the much slower change in region G2 is consistent with the dynamics along the reaction coordinate R depicted in Figure 10. The loss of ionic character manifests itself in several other properties depicted in Figure 11. As the *t*-BuCl recombines, the water potential energy decreases while the water−CCl_4 potential energy increases, indicating that any water molecules that were protruding into the organic phase to solvate the CIP move back to the water side. The time scale for the interface to reach a new equilibrium is slower than the rate of change of the solute electronic structure (as represented by the change in ionic character). The first process involves the collective motions of several water and CCl_4 molecules, while the latter represents the much faster recombination along the R coordinate. We also note that the solute does follow the water back toward the aqueous phase to some extent, as shown by the average solute center-of-mass distance from the Gibbs surface in panel D of Figure 11.

IV. Conclusions

Using classical molecular dynamics simulations with an empirical valence bond model for the *t*-BuCl solute, we have shown that the reduced polarity at the water/CCl_4 interface relative to bulk water causes a destabilization of the *t*-BuCl ionic state resulting in an increase in the activation free energy and reaction free energy to dissociation. The dissociation to ions is

still observed because of the ability of the water to protrude into the CCl_4 region and provide sufficient hydration. This is reminiscent of the local density enhancement at the water liquid/vapor interface[37] and a similar phenomenon in supercritical water.[24] We find that the transition state to dissociation moves to larger values of the *t*-Bu and Cl separation as the *t*-BuCl is moved further into the CCl_4 region. Once the *t*-BuCl is >3 Å into the organic phase, the water density drops significantly and we no longer observe a minimum corresponding to a CIP. The importance of dynamic surface roughness is established by repeating the calculations with an artificially flat interface. We are further investigating this point by examining the dissociation of *t*-BuCl at the water/dichloroethane interface, which provides greater surface roughness and polarity. Recombination dynamics with the *t*-BuCl initiated at the CIP distance show that within 10 ps almost all trajectories become trapped in the covalently bound well, although remaining vibrationally hot. These results may be relevant for observation of ion pair recombination following laser-induced dissociation of adsorbed dye molecules.

Acknowledgment. This work has been supported by a grant from the National Science Foundation (CHE-0345361).

References and Notes

(1) Arai, K.; Ohsawa, M.; Kusu, F.; Takamura, K. *Bioelectrochem. Bioenerg.* **1993**, *31*, 65.
(2) *The Chemistry of Acid Rain: Sources and Atmospheric Processes*; Johnson, R. W., Gordon, G. E., Eds.; American Chemical Society Symposium Series 349; American Chemical Society: Washington, DC, 1987.
(3) Starks, C. M.; Liotta, C. L.; Halpern, M. *Phase Transfer Catalysis*; Chapman & Hall: New York, 1994.
(4) Garcia-Rio, L.; Leis, J. R.; Moreira, J. A. *J. Am. Chem. Soc.* **2000**, *122*, 10325.
(5) Campbell, C. J.; Rusling, J. F. *Langmuir* **1999**, *15*, 7416.
(6) Husein, M. M.; Weber, M. E.; Vera, J. H. *Langmuir* **2000**, *16*, 9159.
(7) Naujok, R. R.; Paul, H. J.; Corn, R. M. *J. Phys. Chem.* **1996**, *100*, 10497.
(8) Uchiyama, Y.; Fujinami, M.; Sawada, T. *J. Phys. Chem. B* **2000**, *104*, 4699.
(9) Warshel, A. *J. Phys. Chem.* **1982**, *86*, 2218.
(10) Hynes, J. T. The theory of reactions in solution. In *The Theory of Chemical Reactions*; Baer, M., Ed.; CRC Press: Boca Raton, FL, 1985; Vol. 4; p 171.
(11) Gertner, B. J.; Wilson, K. R.; Lee, S.; Hynes, J. T. *Faraday Discuss. Chem. Soc.* **1988**, *85*, 297.
(12) Kim, H. J.; Hynes, J. T. *J. Chem. Phys.* **1990**, *93*, 5194.
(13) Bianco, R.; Hynes, J. T. *J. Chem. Phys.* **1995**, *102*, 7864.
(14) Truong, T. N.; Truong, T. T.; Stefanovich, E. V. *J. Chem Phys.* **1997**, *107*, 1881.
(15) Cuma, M.; Schmitt, U. W.; Voth, G. A. *Chem. Phys.* **2000**, *258*, 187.
(16) Reichardt, C. *Solvents and Solvent Effects in Organic Chemistry*, 2nd ed.; Springer-Verlag: Weinheim, 1988.
(17) Ingold, C. K. *Stucture and Mechanism in Organic Chemistry*, 2nd ed.; Cornell University: Ithaca, NY, 1969.
(18) Ogg, R. A.; Polanyi, M. *Trans. Faraday Soc.* **1935**, *31*, 604.
(19) Jorgensen, W. L.; Buckner, J. K.; Huston, S. E.; Rossky, P. J. *J. Am. Chem. Soc.* **1987**, *109*, 1891.
(20) Kim, H. J.; Hynes, J. T. *J. Am. Chem. Soc.* **1992**, *114*, 10508.
(21) Keirstead, W. P.; Wilson, K. R.; Hynes, J. T. *J. Chem. Phys.* **1991**, *95*, 5256.
(22) Kim, H. J.; Hynes, J. T. *J. Am. Chem. Soc.* **1992**, *114*, 10528.
(23) Okuno, Y. *J. Phys. Chem. A* **1999**, *103*, 190.
(24) Westacott, R. E.; Johnston, K. P.; Rossky, P. J. *J. Phys. Chem. B* **2001**, *105*, 6611.
(25) Wang, H.; Borguet, E.; Eisenthal, K. B. *J. Phys. Chem. A* **1997**, *101*, 713.
(26) Zhang, X.; Steel, W. H.; Walker, R. A. *J. Phys. Chem. B* **2003**, *107*, 3829.
(27) Benjamin, I. *Annu. Rev. Phys. Chem.* **1997**, *48*, 401.
(28) Benjamin, I. *J. Chem Phys.* **2004**, *121*, 10223.
(29) Gomes, J. A.; dos Santos, D. J. *Chemphyschem* **2002**, *3*, 946.
(30) Schlossman, M. L. *Curr. Opin. Colloid Interface Sci.* **2002**, *7*, 235.
(31) Steel, W. H.; Walker, R. A. *Nature* **2003**, *424*, 296.
(32) Schweighofer, K. J.; Benjamin, I. *J. Phys. Chem. A* **1999**, *103*, 10274.
(33) Warshel, A.; Weiss, R. M. *J. Am. Chem. Soc.* **1980**, *102*, 6218.
(34) Warshel, A. *J. Phys. Chem.* **1982**, *86*, 2218.
(35) Ando, K.; Hynes, J. T. *J. Phys. Chem. B* **1997**, *101*, 10464.
(36) Day, T. J. F.; Soudackov, A. V.; Cuma, M.; Schmitt, U. W.; Voth, G. A. *J. Chem. Phys.* **2002**, *117*, 5839.
(37) Winter, N.; Benjamin, I. *J. Chem. Phys.* **2005**, *122*, 184717.
(38) Kuchitsu, K.; Morino, Y. *Bull. Chem. Soc. Jpn.* **1965**, *38*, 814.
(39) Benjamin, I. Molecular dynamics methods for studying liquid interfacial phenomena. In *Modern Methods for Multidimensional Dynamics Computations in Chemistry*; Thompson, D. L., Ed.; World Scientific: Singapore, 1998; p 101.
(40) Michael, D.; Benjamin, I. *J. Chem. Phys.* **2001**, *114*, 2817.
(41) Benjamin, I. In *Modern Aspects of Electrochemistry*; Bockris, J. O. M., Conway, B. E., White, R. E., Eds.; Plenum: New York, 1997; Vol. 31; p 115.
(42) Sprik, M.; Klein, M. L. *J. Chem. Phys.* **1988**, *89*, 7556.
(43) Ahlstrom, P.; Wallqvist, A.; Engstrom, S.; Jonsson, B. *Mol. Phys.* **1989**, *68*, 563.
(44) Wallqvist, A. *Chem. Phys. Lett.* **1990**, *165*, 437.
(45) Dang, L. X.; Rice, J. E.; Caldwell, J.; Kollman, P. A. *J. Am. Chem. Soc.* **1991**, *113*, 2481.
(46) Smith, D. E.; Dang, L. X. *J. Chem. Phys.* **1994**, *100*, 3757.
(47) Bader, J. S.; Berne, B. J. *J. Chem. Phys.* **1996**, *104*, 1293.
(48) Morita, A.; Kato, S. *J. Chem. Phys.* **1998**, *109*, 5511.
(49) Small, D. W.; Matyushov, D. V.; Voth, G. A. *J. Am. Chem. Soc.* **2003**, *125*, 7470.
(50) Wallqvist, A. *Chem. Phys.* **1990**, *148*, 439.
(51) Motakabbir, K.; Berkowitz, M. *Chem. Phys. Lett.* **1991**, *176*, 61.
(52) Chang, T. M.; Dang, L. X. *J. Chem. Phys.* **1996**, *104*, 6772.
(53) Benjamin, I. *Chem. Phys. Lett.* **1998**, *287*, 480.
(54) Dang, L. X.; Chang, T. *J. Phys. Chem. B* **2002**, *106*, 235.
(55) Jungwirth, P.; Tobias, D. J. *J. Phys. Chem. A* **2002**, *106*, 379.
(56) Hansen, J.-P.; McDonald, I. R. *Theory of Simple Liquids*, 2nd ed.; Academic: London, 1986.
(57) McQuarrie, D. A. *Statistical Mechanics*; Harper & Row: New York, 1976.
(58) Winstein, S.; Fainberg, A. H. *J. Am. Chem. Soc.* **1957**, *79*, 5937.
(59) Chorny, I.; Vieceli, J.; Benjamin, I. *J. Phys. Chem. B* **2003**, *107*, 229.
(60) Vieceli, J.; Chorny, I.; Benjamin, I. *J. Chem. Phys.* **2002**, *117*, 4532.
(61) Chorny, I.; Benjamin, I. *J. Mol. Liq.* **2004**, *110*, 133.